remote sensing

MDPI

Article

A Global, Multidecadal Carbon Monoxide (CO) Record from the Sounder AIRS/CrIS System

Tao Wang *, Vivienne H. Payne, Evan Manning †, Thomas S. Pagano, Bjorn Lambrigtsen and Ruth Monarrez

NASA Jet Propulsion Laboratory, California Institute of Technology, Pasadena, CA 91011, USA; vivienne.h.payne@jpl.nasa.gov (V.H.P.)
* Correspondence: tao.wang@jpl.nasa.gov
† Now retired.

Highlights

Carbon monoxide (CO)—emitted by fossil-fuel combustion, biomass burning, and wildfires—plays a central role in atmospheric chemistry and serves as a tracer of pollution and fire-related emissions. Since 2000, satellites have provided global CO coverage, but ensuring the long-term consistency of these observations is critical for studying how the Earth's atmosphere is changing. Here we show that CO retrieved from AIRS (launched in 2002) and its successor CrIS (operated since 2011), despite different instruments and algorithms, is consistent enough to form a reliable, multidecadal CO record. The measurements of CO variability agree closely with each other and align well with earlier observations by the MOPITT instrument. This cross-platform robustness reflects the strength and clarity of the CO signal in infrared spectrum. We also find that recent increases in wildfire activity—especially in the Northern Hemisphere—are clearly evident in these satellite CO records. These findings are supported by complementary MODIS fire detections and AIRS near-surface vapor pressure deficit (VPD). With future CrIS missions planned through the 2030s, we can expect 40+ years of continuous space-based CO observations from the U.S. afternoon-orbit hyperspectral sounders.

Abstract

Satellite observations of carbon monoxide (CO) are essential for monitoring global air quality, pollution transport, and climate-related emissions. This study evaluates the continuity and consistency of CO measurements derived from the Atmospheric Infrared Sounder (AIRS) and the Cross-track Infrared Sounder (CrIS), both operating in the thermal infrared band near 4.6 μm. By comparing retrievals from the AIRS Science Team v7 and the CLIMCAPS (Community Long-term Infrared Microwave Combined Atmospheric Product System) algorithms across AIRS and CrIS radiances, we demonstrate that the interannual CO variability is consistent across instruments and algorithms. These findings are validated using the long-term MOPITT record. Additionally, we show that mid-tropospheric CO variabilities correspond with fire detections from MODIS and surface vapor pressure deficit (VPD) anomalies, indicating a rise in wildfire activity in the Northern Hemisphere. The results shown here provide confidence in the utility of a combined AIRS/CrIS CO record. With the scheduled continuation of CrIS observations through future JPSS platforms, the combined CO record from U.S. hyperspectral sounders in the afternoon orbit is set to continue to 2045 and beyond, providing a possible means to quantify trends and interannual variability over multiple decades.

Check for updates

Academic Editor: Carmine Serio

Received: 20 October 2025
Revised: 5 December 2025
Accepted: 15 December 2025
Published: 19 December 2025

Copyright: © 2025 by the authors. Licensee MDPI, Basel, Switzerland. This article is an open access article distributed under the terms and conditions of the Creative Commons Attribution (CC BY) license.

Keywords: satellite; carbon monoxide; CO; sounder; interannual variability; annual cycle; frequent wildfires; global warming

1. Introduction

Carbon monoxide (CO) is a colorless, odorless gas that plays a key role in atmospheric chemistry. Tropospheric CO below the 100 hPa level primarily reflects surface emissions from both anthropogenic and natural sources. Anthropogenic sources include the incomplete combustion of fossil fuels (e.g., coal, gas, and oil), biomass burning [1], and waste incineration. Natural sources include wildfires, the oxidation of hydrocarbons such as methane (CH_4) [2], volcanic emissions, and even oceanic emissions [3]. Once released into the atmosphere, CO can persist for several months, making it a valuable tracer for studying long-range transport of pollutions and biomass burning plumes [4–6]. In some cases, CO can even be transported into the lower stratosphere [7,8].

Ground-based CO measurements offer important local data but lack the coverage needed to capture global and regional patterns. Satellite-based instruments, in contrast, can provide global CO observations with consistent spatial and temporal resolution. This is especially important for evaluating impacts of emissions from wildfires, which have become more frequent and severe due to climate warming [9].

Tropospheric CO can be observed via satellite remote sensing in the near-infrared (NIR, 2.3–2.4 μm or 4350–4170 cm^{-1}) and thermal infrared (TIR, 4.4–5.2 μm or 2270–1920 cm^{-1}) spectral bands. NIR-only instruments, offering sensitivity to total column CO, include the Scanning Imaging Absorption Spectrometer for Atmospheric Cartography (SCIAMACHY) on Envisat (2002–2012) [10] and the Tropospheric Ozone Monitoring Instrument (TROPOMI) on Sentinel 5p (2017–present) [11].

TIR-only instruments offer sensitivity to CO primarily in the free troposphere, with some limited profiling capability, depending on spectral resolution. One advantage of TIR measurements is that retrievals of CO in the presence of smoke are not significantly affected by scattering for infrared observations at wavelengths ~4.6 μm. This is because Rayleigh scattering, which scales inversely with wavelength to the fourth power ($\propto \lambda^{-4}$), is negligible at these wavelengths; while Mie scattering becomes significant only for particles larger than approximately $\lambda/\pi \approx 1.5$ μm (e.g., [12]). In contrast, the size distribution of biomass-burning smoke particles typically peaks near 0.3 μm (e.g., [13]).

The Advanced Earth Observing Satellite Interferometric Monitor for Greenhouse Gases (ADEOS IMG) [14], which operated from 1996 to 1997, and the Tropospheric Emission Spectrometer [15], which operated from 2004 to 2018, were specifically designed for measurements of atmospheric composition. The TIR hyperspectral sounders in the current program of record have been designed as meteorological sounders but can also provide long-term measurements of CO. Instruments in this category providing CO measurements include those in low earth orbit (LEO) such as the Atmospheric Infrared Sounder (AIRS) on Aqua (e.g., [16]), the Cross-track Infrared Sounders (CrIS) (e.g., [17–19]), the Infrared Atmospheric Sounding Interferometers (IASI) (e.g., [20,21]) and the Hyperspectral Infrared Atmospheric Sounders (HIRAS) [22], as well as those in geostationary (GEO) orbits such as the Geostationary Interferometric Infrared Sounder (GIIRS) [23] and the Meteosat Third-Generation Infrared Sounder (MTG-IRS) [24].

Satellite measurements of CO have been utilized extensively in a wide range of studies of the earth system. For example, satellite CO measurements have provided key insight into fire emissions and their changes over time. This includes biomass burning in the tropics (e.g., [25,26]), as well as wildfires at mid- and high latitudes (e.g., [27–30]). Satellite

CO records have also been widely used for the top-down estimation of anthropogenic emissions of CO at local (e.g., [31]), regional (e.g., [32]), and global (e.g., [33]) scales, and to identify shifting patterns in global CO linked to human activity.

Buchholz et al. [34], in an analysis of the MOPITT TIR-only CO record between 2002 and 2018, showed an overall decreasing trend in global CO concentrations, consistent with previous studies. This work showed consistency in hemispheric seasonality and interannual variability in the MOPITT TIR record and those from other LEO hyperspectral TIR sounders (TES, AIRS, IASI-A/B, and SNPP-CrIS). They observed a deceleration in the global CO trend in the latter half of this period compared to the earlier half, attributed to the atmospheric impact of air quality management policies. However, they noted that local contributions from human pollution or fire emissions can locally counteract the global downward trend in CO and may also have hemispheric impacts through subsequent transport, highlighting the importance of continued monitoring of changes in CO, particularly in light of climate-driven positive fire trends.

MOPITT was officially turned off on 1 February 2025, after 25 years of operation, leaving a legacy of key contributions to the understanding of atmospheric chemistry and emission sources. *Buchholz* et al. [34] have already pointed to the viability of the continuation of the record with meteorological TIR sounders. Here, we evaluate the overall consistency between extended records from the U.S. meteorological LEO sounders, AIRS and CrIS, and the MOPITT record over the 2002–2025 period. We focus on the AIRS v7, CLIMCAPS-Aqua (also AIRS), CLIMCAPS-SNPP (CrIS), and CLIMCAPS-JPSS1 (CrIS) Level 2 data products. All these products, which are produced from Level 2 cloud-cleared radiances on the 45 km field of regard (see section below), are publicly available for the entire length of the AIRS and CrIS records.

Multi-decadal satellite records of CO can support ongoing research into atmospheric chemistry and the impacts of wildfire trends on atmospheric composition. This study aims to assess the continuity of CO records across AIRS and CrIS. Section 2 introduces the AIRS/CrIS instrument and their retrieval algorithms; Section 3 demonstrates the annual cycle and consistent interannual variabilities of CO across different instruments and algorithms; Section 4 presents the more frequent and intense wildfires shown in those records.

2. The AIRS/CrIS Instrument and Data

This study analyzes CO retrievals from two main sources: the AIRS Science Team (AST) algorithm that processes radiances from the AIRS instrument, and the CLIMCAPS (Community Long-term Infrared Microwave Combined Atmospheric Product System) algorithm [17] that processes radiances from both AIRS and CrIS instruments. Both AIRS and CrIS include a subset of hyperspectral infrared (IR) channels sensitive to the CO TIR absorption band in the 2040–2250 cm^{-1} (4.8–4.4 μm) range.

AIRS, launched in 2002 aboard NASA's Aqua satellite, is a grating spectrometer that provides high-resolution wide spectral coverage between 650 and 1613 cm^{-1} and between 2181 and 2665 cm^{-1} (6.19–15.39 μm and 3.75–4.58 μm). Note that with a resolving power R of ~1200 for the AIRS grating spectrometer, at different wave number $\tilde{\nu}$, the spectral resolution (wave spacing) $\Delta\tilde{\nu}$ is different. For example, at $\tilde{\nu}$ = ~2200 cm^{-1} for the CO band, the spectral resolution is $\Delta\tilde{\nu} = \tilde{\nu}/R = 2200\ cm^{-1}/1200 \approx 1.8\ cm^{-1}$. The instrument observes a 3 by 3 array of 15 km footprints within a 45 km field of regard [35]. The radiance spectra enable observations of temperature and water vapor profiles as well as composition profiles. AIRS observes CO primarily in the TIR band centered around ~4.6 μm, with sensitivity to variations in the middle to upper troposphere (e.g., [36–38]. AIRS has limited sensitivity to CO near the surface, especially under cloudy conditions [39].

For the past two decades, AIRS CO products have been extensively used to study regional and global CO emissions from biomass burning, industrial sources, and urban pollution. By combining AIRS, MOPITT, TES, and IASI measurements, *Worden* et al. [40] derived a consistent decadal record of total column CO from 2000 to 2011, revealing a modest hemispheric decline of about 1%/year and statistically significant decrease over eastern China, the eastern United States, and Europe. *Zhang* et al. [41] used 2003–2017 AIRS and MOPITT data to characterize spatial and temporal variations in CO total column over Asia and assess how these variations respond to biomass burning. *Yurganov and Rakitin* [30] used 20 years of AIRS TIR CO observations (2002–2021) with a simple two-box mass-balance model to derive the top-down estimates from biomass burning north of 30°N, with results that closely track those from GFED4c (Global Fire Emissions Database, [42]) in both seasonality and interannual variability.

To ensure continuity beyond the AIRS mission, NASA and NOAA have deployed the CrIS instrument onboard a series of polar-orbiting satellites: Suomi-NPP (since 2011), JPSS-1 (since 2017), and JPSS-2 (since 2022), with future launches planned through 2032. CrIS is a Fourier transform spectrometer that continues the observational legacy of AIRS. CrIS also observes a 3 by 3 array of 15 km footprints within a 45 km field of regard.

Figure 1a illustrates all 2378 AIRS channels (blue bars on the top) and the 36 selected for CO retrievals (red bars), alongside all 2223 CrIS full-spectral-resolution (FSR) channels (green bars) and the 35 selected for CO retrievals (orange bars). The AIRS grating spectrometer has a spectral resolution of ~1.8 cm^{-1} full width at half maximum (FWHM) in the CO spectral range, while CrIS provides finer resolution at ~0.625 cm^{-1}. These channels are compared to CO absorption lines from the HITRAN database (black), assuming a standard atmospheric profile with temperature of 264 K, pressure of 500 hPa, and an absorption path length of 15 cm (data sourced from www.SpectraPlot.com/absorption, accessed on 4 December 2025).

A close-up in Figure 1b highlights the strong CO absorption features between 2050 and 2250 cm^{-1}. Two distinct absorption peaks are centered around 2110 cm^{-1} and 2172 cm^{-1}. AIRS (in blue) covers the right portion of the second peak with 36 channels between 2181 and 2221 cm^{-1} (4.50–4.58 μm), while CrIS (in green) spans almost the entire second peak with 35 channels between 2155 and 2191 cm^{-1} (4.56–4.64 μm).

Several different retrieval algorithms have been applied to both AIRS and CrIS radiances to derive temperature, water vapor, and trace gas profiles. These include algorithms that start from "cloud-cleared" [43] Level 2 radiances on the 45 km field of regard (e.g., [17,36,44,45]) and those that start from Level 1B radiances on the native 15 km single footprints (e.g., [19,46–48]). In this work, we focus on the AIRS v7, CLIMCAPS-Aqua (also AIRS), CLIMCAPS-SNPP (CrIS), and CLIMCAPS-JPSS1 (CrIS) Level 2 data products. These products, which are produced from Level 2 cloud-cleared radiances on the 45 km field of regard, are publicly available for the entire length of the AIRS and CrIS records.

The CO retrieval in the AIRS version 7 retrieval algorithm carries on the legacy from the AIRS version 5 algorithm described in *McMillan* et al. [16], but with an updated *a priori.* AIRS v7 uses monthly climatological CO profiles as the *a priori*, differentiated for the Northern and Southern Hemispheres. The *a priori* profiles are derived from MOPITT v4 climatology, varying with month, longitude, and pressure, and are identified in the retrieval system as COfgtype = 3. Due to AIRS's mid-tropospheric sensitivity (primarily 300–600 hPa), retrievals at surface and high altitudes tend to relax toward the prior. This behavior is confirmed in averaging kernel diagnostics [38]. Because of these limitations, AIRS version 7 no longer provides total column CO as a standard product, given that such estimates are strongly influenced by the prior.

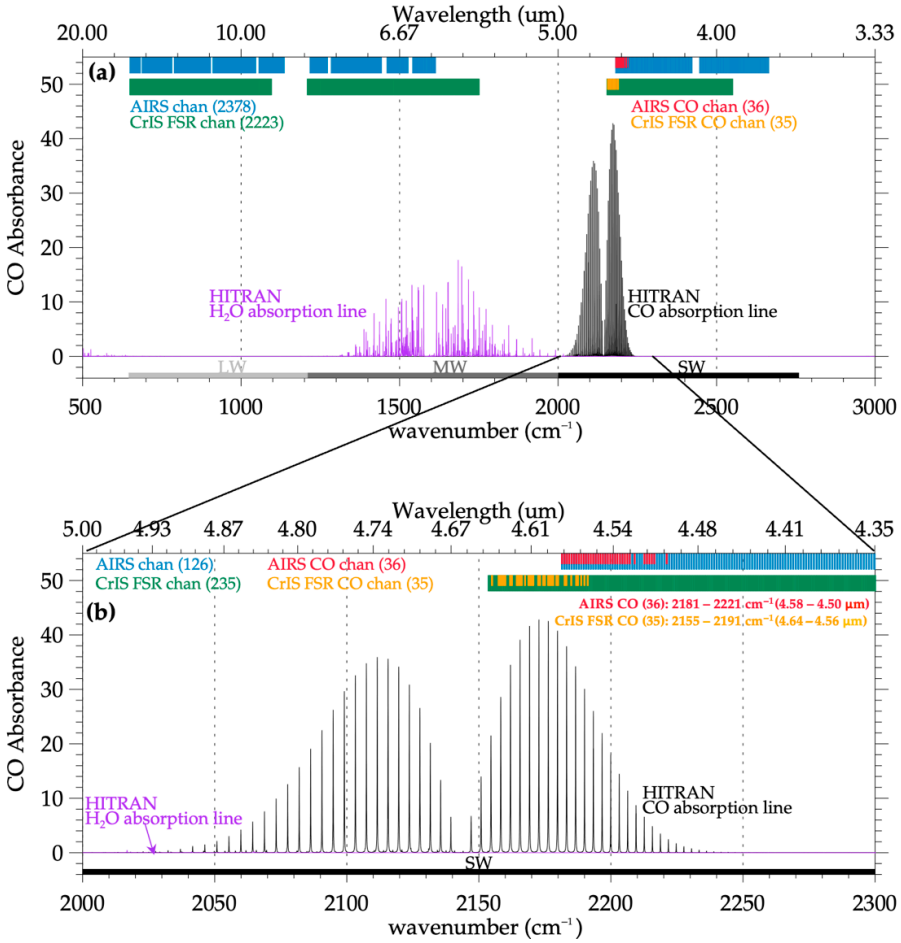

Figure 1. (**a**) Spectral coverage of AIRS (blue: all channels; red: CO channels) and CrIS FSR (green: all channels; orange: CO channels) overlaid with CO (black) and H_2O (purple) absorption features from HITRAN. (**b**) Zoom-in on the 2000–2300 cm^{-1} range, highlighting the peak CO absorption lines. Absorption calculated using HITRAN for a standard atmosphere with T = 264 K, P = 500 hPa, and a 15 cm path length (via SpectraPlot.com, accessed on 4 December 2025).

CLIMCAPS is a cross-platform retrieval system developed to create long-term, consistent atmospheric profiles using data from multiple instruments—including AIRS/AMSU on Aqua and CrIS/ATMS on SNPP and JPSS satellites. When retrieving CO, CLIMCAPS-Aqua processes AIRS radiances using the legacy AIRS v5-based retrieval algorithm (similar to AIRS v7) but employs a different static *a priori* for CO (COfgtype = 2). This blends Air Force Geophysics Laboratory (AFGL) standard profile [49] for the lower atmosphere and MOPITT v3 climatology for upper levels [16].

Both AIRS v7 and CLIMCAPS-Aqua CO retrievals have been validated against in situ CO measurements from the five HIAPER Pole-to-Pole Observations (HIPPO) campaigns conducted between 2009 and 2011 [38]. While both use similar retrieval algorithms and the same AIRS radiances, CLIMCAPS-Aqua underestimate CO by at least 10–20% relative to AIRS v7, which is largely attributed to the older, static *a priori* used in CLIMCAPS-Aqua. Nevertheless, both products capture the interannual variability of CO that closely aligns with MOPITT trends, as shown in Section 3.

CLIMCAPS also processes radiances from the CrIS instrument onboard SNPP and JPSS-1. In this study, we include only full-spectral-resolution (FSR) data from CrIS (δ = 0.625 cm^{-1}), which provides improved vertical sensitivity over the nominal spectral resolution (NSR, δ = 2.5 cm^{-1}) [50]. Like CLIMCAPS-Aqua, these CrIS-based products use the same legacy retrieval algorithm, but with an updated hybrid *a priori* (COfgtype = 4)

that combines the AFGL and MOPITT v4 climatology. This hybrid *a priori* applies more weight to the top-of-atmosphere (TOA) conditions to improve profile performance in the upper troposphere.

Table 1 summarizes the details of CO products from the AIRS v7 and CLIMCAPS algorithms using either AIRS radiances (CLIMCAPS-Aqua) or CrIS radiances (CLIMCAPS-SNPP and CLIMCAPS-JPSS). Note that, for CO retrievals, CLIMCAPS and AIRS v7 algorithms are largely based on the same algorithm that has not been changed much since the legacy AIRS v5 algorithm (*N. Smith*, *personal communication*). Therefore, AIRS v7 and CLIMCAPS-Aqua CO are based on the same AIRS radiances and a largely similar algorithm but differ in their *a priori* assumptions; CLIMCAPS-Aqua and CLIMCAPS-SNPP CO use the same retrieval algorithm but are driven by different radiances (AIRS vs. CrIS) with distinct *a priori*. By contrast, CLIMCAPS-SNPP and CLIMCAPS-JPSS1 CO products are based on the same algorithm and the same *a priori*, but differ only in that they use CrIS radiances from different satellites (SNPP vs. JPSS1). Given the shared algorithms and radiances, we infer that most of the differences among CO products are attributable to the differences in their *a priori* assumptions.

Table 1. AIRS/CrIS CO product details.

L2 CO Product \ Feature	Algorithm	Input Radiance	*A Priori*	*A Priori* Details	Time Period
AIRS v7	AIRS Science Team v7	AIRS	COfgtype = 3	MOPITT v4 clim. NH/SH	2003–2025
CLIMCAPS-Aqua	CLIMCAPS	AIRS	COfgtype = 2	AFGL_MOPP, static profile	2003–2025
CLIMCAPS-SNPP	CLIMCAPS	CrIS	COfgtype = 4	AFGL_MOPP + MOPITT v4 clim. NH/SH	2015–2021
CLIMCAPS-JPSS1	CLIMCAPS	CrIS	COfgtype = 4	AFGL_MOPP + MOPITT v4 clim. NH/SH	2018–2025

For independent validation, we compare the CO retrievals from AIRS v7 and CLIMCAPS to the MOPITT Version 9 CO [51]. MOPITT TIR channels (centered near 4.7 μm or ~2150 cm^{-1}) are most sensitive to CO in the mid-troposphere (~400–500 hPa), closely matching the peak sensitivity of AIRS and CrIS. This study primarily utilizes MOPITT Level 3 daily mean CO from TIR (MOP03T) gridded at 1° × 1° resolution, which reduces random retrieval noise compared to Level 2 data. For comparison, we also include the MOPITT joint infrared retrieval (TIR + NIR, MOP03J) that makes use of the greatest sensitivity to CO in the lower troposphere and offers the greatest vertical resolution but is subject to larger random retrieval errors and potential bias drift due to the involvement of NIR retrievals [51,52]. However, note that MOPITT's NIR retrievals, while useful for total column CO, are limited to daytime observations over land due to their dependence on reflected sunlight. Compared to the spectral resolution of AIRS (~1.8 cm^{-1}) and CrIS (~0.625 cm^{-1}), MOPITT's effective spectral resolution for CO is coarser at ~2–3 cm^{-1} FWHM.

Sensitivity to CO from AIRS, CrIS, and MOPITT can be better understood in Figure 2, which compares the vertical sensitivity—the so-called "verticality" (sum of each row of averaging kernel, upper row) and degree of freedom (DoF, lower row). The verticality is the sum of each row of averaging kernels, with value near unity indicating that the information comes primarily from the measured radiances at that level. The black dots mark the average altitudes where verticality peaks (most information contents available), which is at the mid-troposphere 400–500 hPa for all instruments. CLIMCAPS-JPSS1 shows higher verticality and DoF due to its finer spectral sampling and lower noise in the 4.7 μm CO band.

Both verticality and DoF peak in the mid-latitudes near 30°N/S. This reflects a combination of strong surface-atmosphere thermal contrast and pronounced tropospheric temperature gradients in these latitudes, which enhance the sensitivity of TIR radiances to CO, together with generally less deep convective clouds than in the deep tropics, which essentially attenuates TIR signal. In addition, anthropogenic and biomass burning sources in the midlatitudes produce large horizontal and vertical CO gradients, further increasing the retrievable signal. In contrast, deep convective clouds in the equatorial belt and weak

surface–atmosphere thermal contrast at high latitudes both reduce the effective sensitivity and hence the information content of the retrievals.

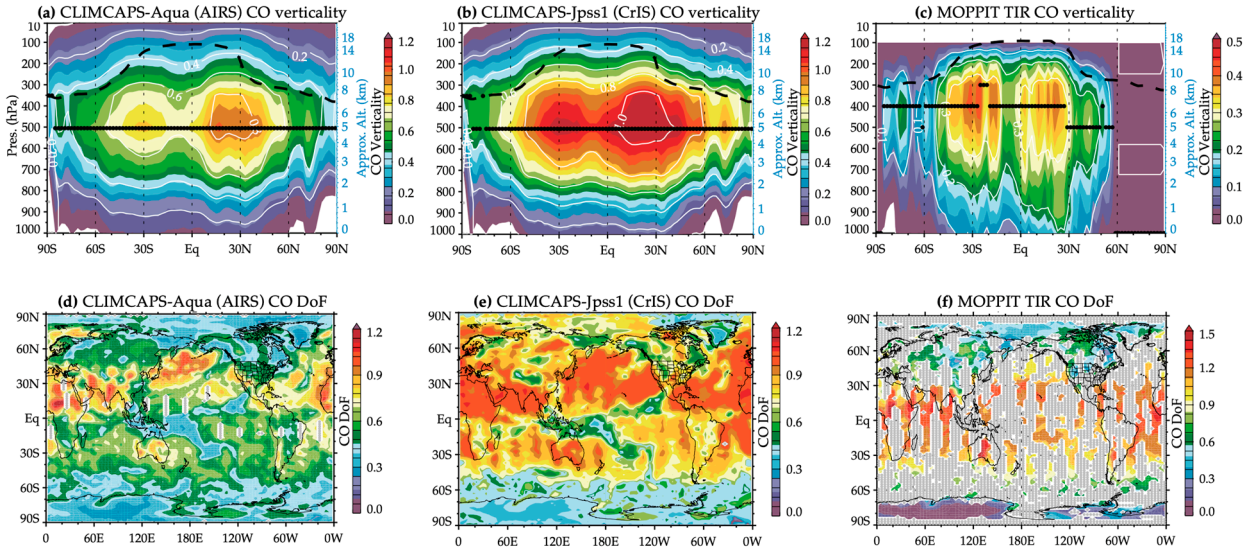

Figure 2. The vertical sensitivity—verticality (**a**–**c**) and the degree of freedom (DoF, (**e**,**f**)) of CO retrievals from CLIMCAPS-Aqua using AIRS radiances (**a**,**d**), CLIMCAPS-JPSS1 using CrIS radiances (**b**,**e**), and MOPITT thermal infrared TIR (**c**,**f**). In upper row, the thick black dots mark the maximum verticality in a profile, which represents where the information peaks; the black dashed lines mark the local thermal tropopause following the WMO definition.

To ensure consistency in the intercomparisons, daily CO datasets from AIRS v7, CLIMCAPS, and MOPITT were homogenized to 4° longitude × 2° latitude grids. AIRS v7 and CLIMCAPS report CO on 100 pressure layers, while MOPITT provides CO profiles on 9 pressure layers. To emphasize the consistency of the long-term CO records, we primarily present time-varying Hovmöller diagrams (time–height and time–latitude) and corresponding time series. The interannual CO anomalies are calculated by removing the mean seasonal cycle, which is computed as the multi-year mean for each calendar day over the analysis period. For example, all 1 January data are differenced from the 1 January mean for 2014–2024, all 2 January data are subtracted from the 2 January mean, and so forth. Removing this dominant seasonal signal (annual cycle) makes the long-term trends and extreme events more apparent in the data.

With MOPITT ending operations in early 2025 and AIRS expected to conclude by 2026, on the U.S. side, CrIS has become the primary instrument for extending TIR CO observations into the next decades. Given that CrIS is now flying on SNPP, JPSS-1, and JPSS-2—with JPSS-4 and JPSS-3 launches scheduled for 2027 and 2032, respectively—a 40+ year record of CO is achievable if consistency across these systems can be demonstrated.

3. Annual Cycle and Interannual Variabilities of CO from Sounder Systems

As discussed above, we might expect differences in CO magnitude among the four TIR sounder products due to differences in prior profiles. Figure 3 compares the daily evolution of mean CO over the Northern Hemisphere mid-latitude (50–75°N) for the last decade (2014–2025). Here, CO retrievals from AIRS v7 (Figure 3b) and CLIMCAPS-Aqua (Figure 3c)—which both used AIRS radiances but with different *a priori*—are compared to CO from CLIMCAPS-SNPP FSR (Figure 3d) and CLIMCAPS-JPSS1 FSR (Figure 3e)—which both used CrIS radiances and the same *a priori*. All four datasets are evaluated against MOPITT TIR CO (MOP03T, Figure 3a) as a transfer standard.

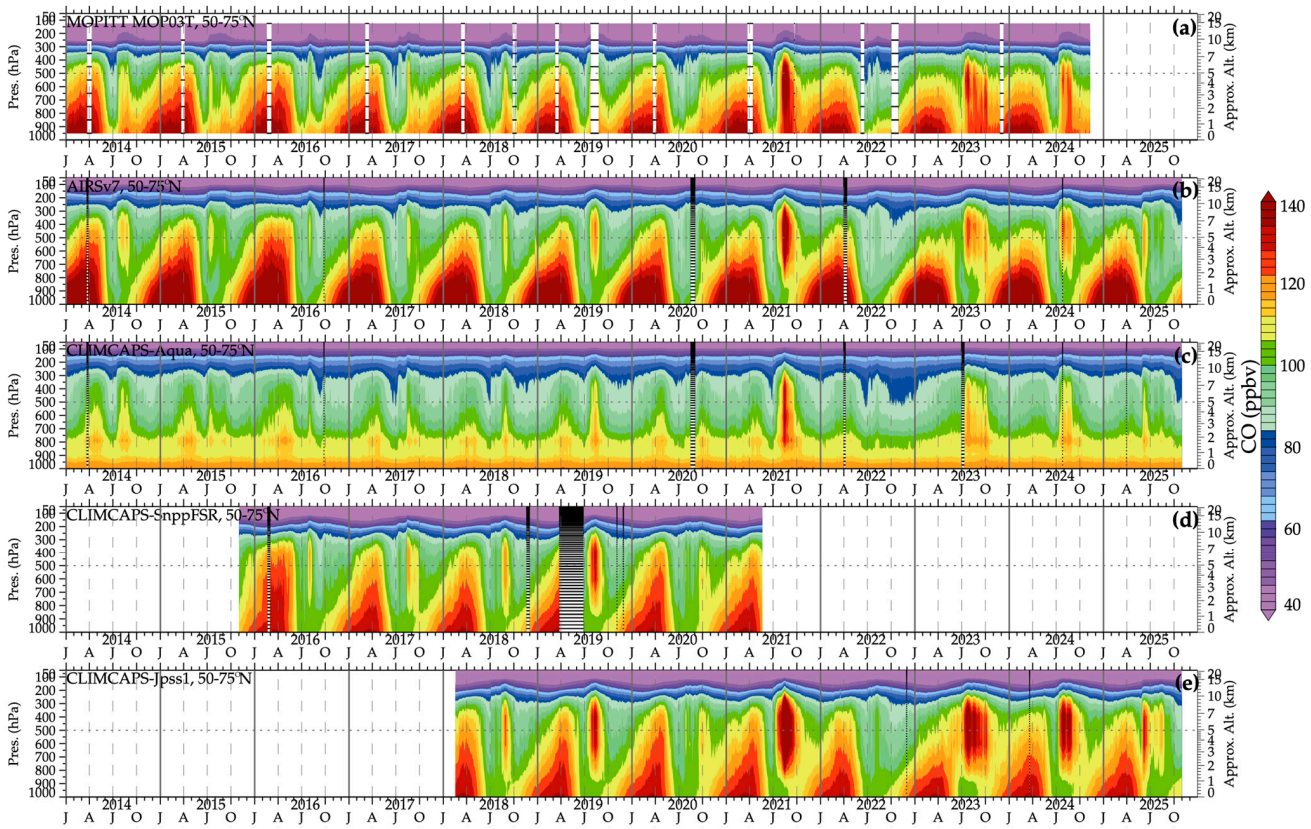

Figure 3. Annual cycle of daily mean CO profiles averaged over 50–75°N for 2014–2024 from (**a**) MOPITT TIR, (**b**) AIRS v7 IR-only, (**c**) CLIMCAPS-Aqua IR-only, (**d**) CLIMCAPS-SNPP FSR, and (**e**) CLIMCAPS-JPSS1 FSR. These panels illustrate the influence of different instruments, algorithms, and *a priori* assumptions on retrieved CO. On each panel, black dots for any day indicate missing data on that day; horizonal, black dotted lines in all panels mark the 500 hPa level, where AIRS/CrIS/MOPITT is most sensitive to CO. For each year, labels "J", "A", "J", "O" on x-axis represents "January", "April", "July", and "October", respectively.

Compared to MOPITT TIR CO, AIRS v7 overestimates CO from the surface to the lower troposphere by 10–15%. Due to a lack of sensitivity, the high-biased CO directly comes from its first guess (COfgtype = 3) that does not vary with time. This can also be seen in Figure 4, where the interannual variability in AIRS v7 CO is rather small, below ~800 hPa.

Conversely, CLIMCAPS-Aqua (Figure 3c) systematically underestimates CO by at least 15–25% across most altitudes when compared to MOPITT. Although it uses a similar retrieval framework as AIRS v7, it employs an older, static *a priori* (COfgtype = 2), which contributes to the observed low bias. These differences have been previously documented in the AIRS/CLIMCAPS-Aqua Level 2 CO validation report [38]. The CLIMCAPS retrieval for CO has heritage from AIRS v5; therefore, the major differences are mostly caused by the different prior used (COfgtype = 2). This has been discussed in detail in the AIRS v7 and CLIMCAPS-Aqua CO Level 2 test report [38].

CLIMCAPS-SNPP and CLIMCAPS-JPSS1 (Figure 3d,e) provide highly consistent results. This agreement is attributed to their use of the same retrieval algorithm applied to the same type of CrIS radiances, coupled with an identical hybrid *a priori* (COfgtype = 4). Additionally, CrIS's higher spectral resolution (δ = 0.625 cm^{-1}) compared to AIRS (~1.8 cm^{-1}) and MOPITT (~2–3 cm^{-1}) enhances its ability to resolve vertical CO structures, particularly during the Northern Hemisphere fire season (e.g., August–October of 2023 and 2024), as evident in the JPSS1 results.

Despite the significant differences in absolute CO values across the products, the interannual variability remains remarkably consistent. Figure 4 demonstrates this by presenting anomalies in 50–75°N (most of boreal forest) CO profiles after removing the daily mean annual cycle (computed over 2018–2023) from each dataset. Due to data availability, the CLIMCAPS-SNPP record only extends through mid-2021.

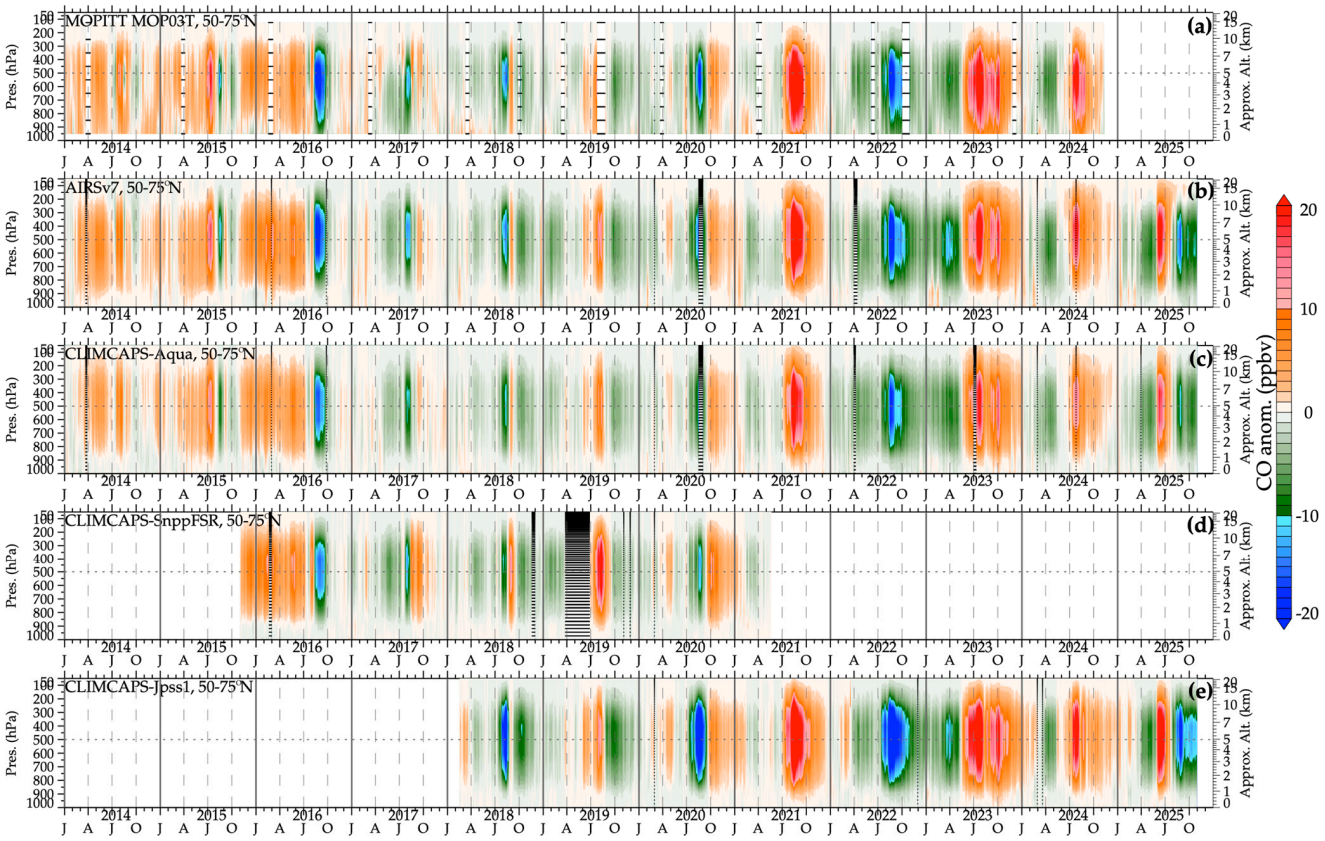

Figure 4. Interannual variability in daily mean CO profiles over 50–75°N for 2014–2024 from (**a**) MOPITT TIR, (**b**) AIRS v7 IR-only, (**c**) CLIMCAPS-Aqua IR-only, (**d**) CLIMCAPS-SNPP FSR, and (**e**) CLIMCAPS-JPSS1 FSR. The 500 hPa level, where thermal IR is most sensitive to CO, is highlighted by a dotted line for each panel. Interannual variability is calculated by removing mean annual cycle 2018–2023 from each dataset. Note that CLIMCAPS-SNPP data ends in mid-2021. Black dots indicate missing data; black dotted lines mark the 500 hPa level, where AIRS/CrIS/MOPITT is most sensitive to CO. For each year, labels "J", "A", "J", "O" on x-axis represents "January", "April", "July", and "October", respectively.

All datasets reveal a general decline in background CO concentrations over the study period. This overall downward trend in CO is consistent with previous studies that were based on shorter records ([34,40]). Bottom-up inventories, such as the Emissions Database for Global Atmospheric Research (EDGAR, 2024, https://edgar.jrc.ec.europa.eu/index.php/dataset_ap81, accessed on 14 December 2025) and the Community Emissions Data System (CEDS, [53]), show that anthropogenic emissions of CO in high-income economies have decreased over the time period of this study, thanks to higher energy efficiency and the implementation of new technology and abatement measures. This has resulted in a downward trend in global anthropogenic CO emissions overall.

Extending the AIRS/CLIMCAPS-Aqua and MOPITT results to the previous decade, they also capture the significant CO dip associated with the 2008–2009 global economic downturn, when reductions in industrial activity, transportation, and shipping led to a

measurable dip in CO emissions (Figures 27 and 29 in *Wang* et al., 2022 [37]; Figures 15 and 16 in *Wang* et al. 2024 [38]).

Meanwhile, an increase in the frequency and intensity of wildfire-related CO plumes is observed, particularly over the past decade. These events are well-captured by AIRS, CLIMCAPS, and MOPITT, and correspond to major documented wildfires, including the 2015–2016 Indonesian peat fires [54], the 2021 Russian wildfires [30], the 2023 Canadian wildfires [27], and the 2024 California, Canadian, and Russia fires (see also Figure 5).

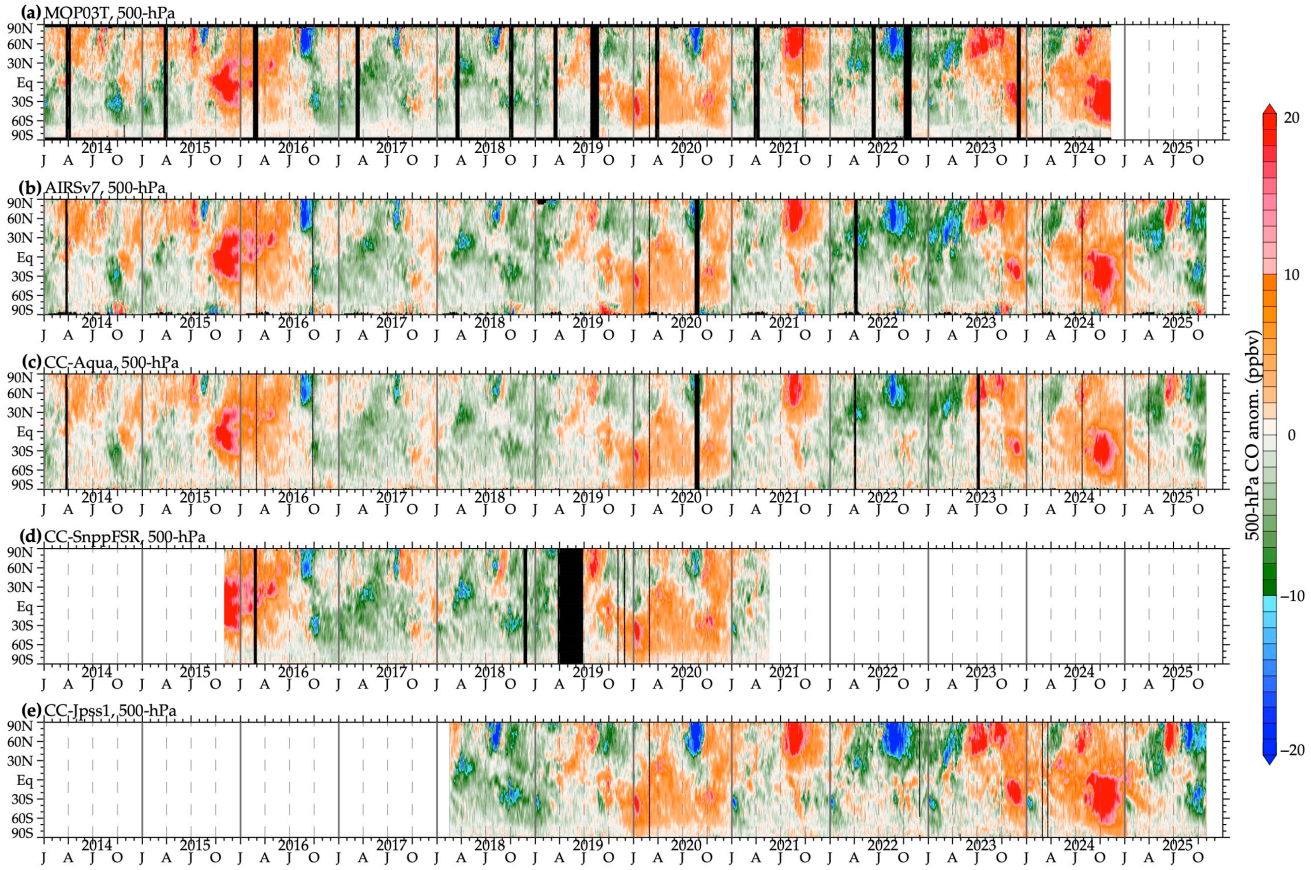

Figure 5. Interannual variability in 500 hPa CO zonal mean from (**a**) MOPITT TIR (MOP03T), (**b**) AIRS v7, (**c**) CLIMCAPS-Aqua, (**d**) CLIMCAPS-SNPP FSR, and (**e**) CLIMCAPS-JPSS1 FSR for 2014–2025. The interannual variabilities of CO is calculated by removing daily annual cycles between 2018–2023. Black dots indicate missing data. For each year, labels "J", "A", "J", "O" on x-axis represents "January", "April", "July", and "October", respectively.

The robustness of mid-tropospheric CO variability is not limited to the Northern Hemisphere mid-latitudes. At 500 hPa—the level at which both AIRS and CrIS exhibit peak sensitivity—CO anomalies are consistent across all latitudes when compared to MOPITT. Figure 5 illustrates this agreement among AIRS, CLIMCAPS, and MOPITT for 500 hPa CO anomalies, showing strong temporal coherence across the globe. Hotspots are observed across boreal regions in North America and Eurasia, as well as in tropical regions like the Amazon, Central Africa, and Southeast Asia. Prominent wildfires reflected in Figure 5 include the 2015–2016 Indonesian fires (tropics and NH mid-latitudes) [54], the 2021 Russian fires [30], and the 2023 Canadian wildfires [27]. In 2024, sustained positive CO anomalies across both North and South America the whole year long reflect the widespread impact of wildfires, including the Canadian fire, the California park fire, and the mega-colossal series of wildfires from South America due to severe drought across Brazil, Peru, Bolivia, and Colombia (e.g., [55]).

A closer look at the 500 hPa CO and their anomalies for a high-CO month (August 2021) and a low-CO month (August 2022) is shown in Figure 6. Although CO absolute magnitudes differ across datasets, their spatial patterns are broadly consistent (Figure 6a), with elevated CO associated with the 2021 wildfires in boreal North America and boreal Eurasia, which were accompanied by record-high CO_2 emissions [56], and relatively low CO in 2022, largely reflecting persistent emissions over Africa. After removing the 2018–2023 annual cycle, the anomaly maps from all datasets exhibit strikingly similar structures, reinforcing that the measured CO show broad consistency for AIRS/CrIS/MOPITT.

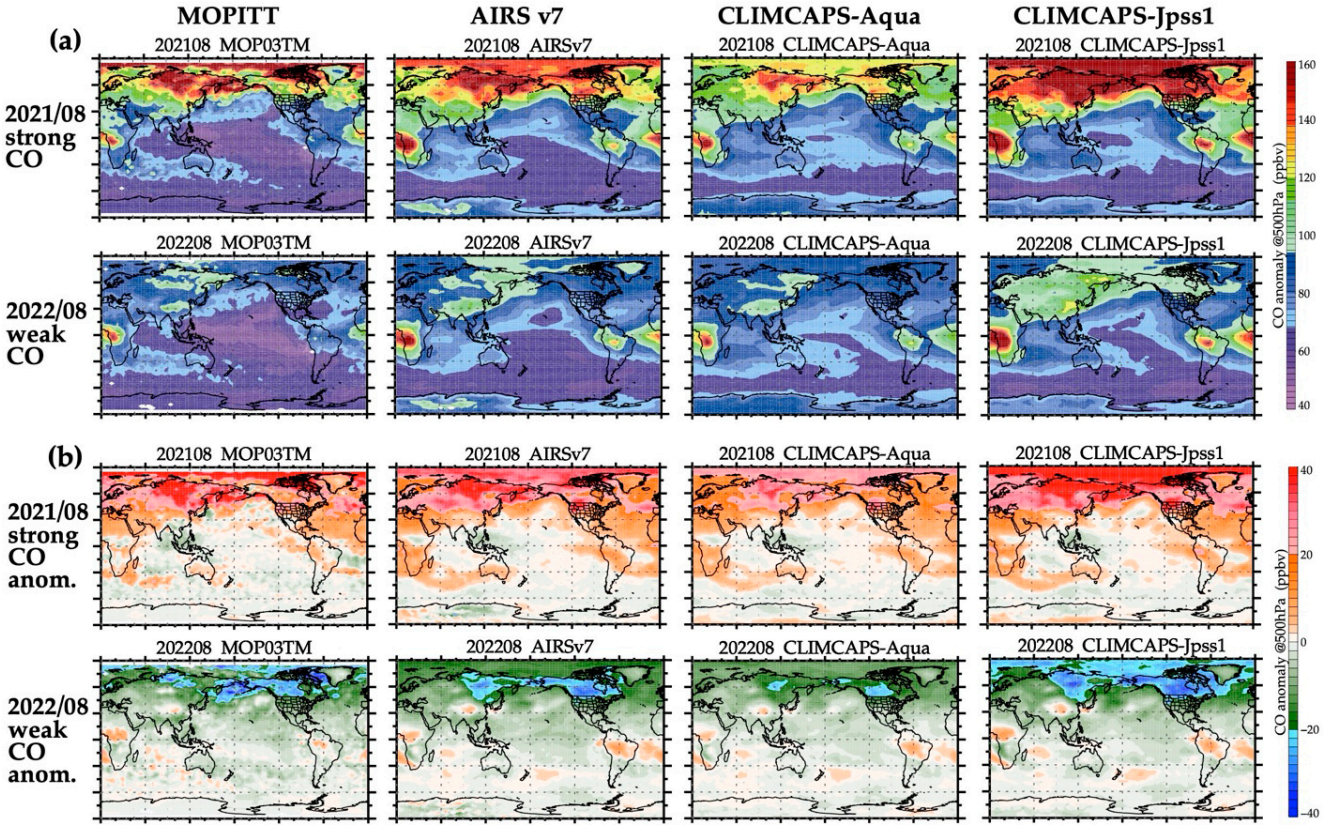

Figure 6. The 500 hPa CO distributions from MOPITT TIR (**left column**), AIRS v7 (**second column**), CLIMCAPS-Aqua (**third column**), and CLIMCAPS-JPSS1 FSR (**right column**) during a high-CO month (August 2021, top two rows) compared to a low-CO month (August 2022, bottom two rows), shown on (**a**) CO magnitudes and (**b**) CO anomalies. The CO anomaly is calculated by removing annual cycles between 2018–2023.

Figure 7 shows the time series of both 500 hPa CO anomalies and total column CO anomalies averaged in different latitude bands. Again, the 500 hPa CO anomalies from AIRS v7, CLIMCAPS-Aqua, CLIMCAPS-SNPP, and CLIMCAPS-JPSS1 all agree with that from MOPITT TIR. Moreover, the variability of 500 hPa CO from AIRS/CrIS/MOPITT closely tracks the variability of MOPITT-reported total column CO (in mol/cm^2, right *y*-axis), whether derived from TIR-only or TIR + NIR retrievals. This indicates that surface-level anthropogenic emissions play a relatively minor role in driving interannual variability at the global scale. Instead, large-scale wildfires emerge as the dominant source of year-to-year CO anomalies.

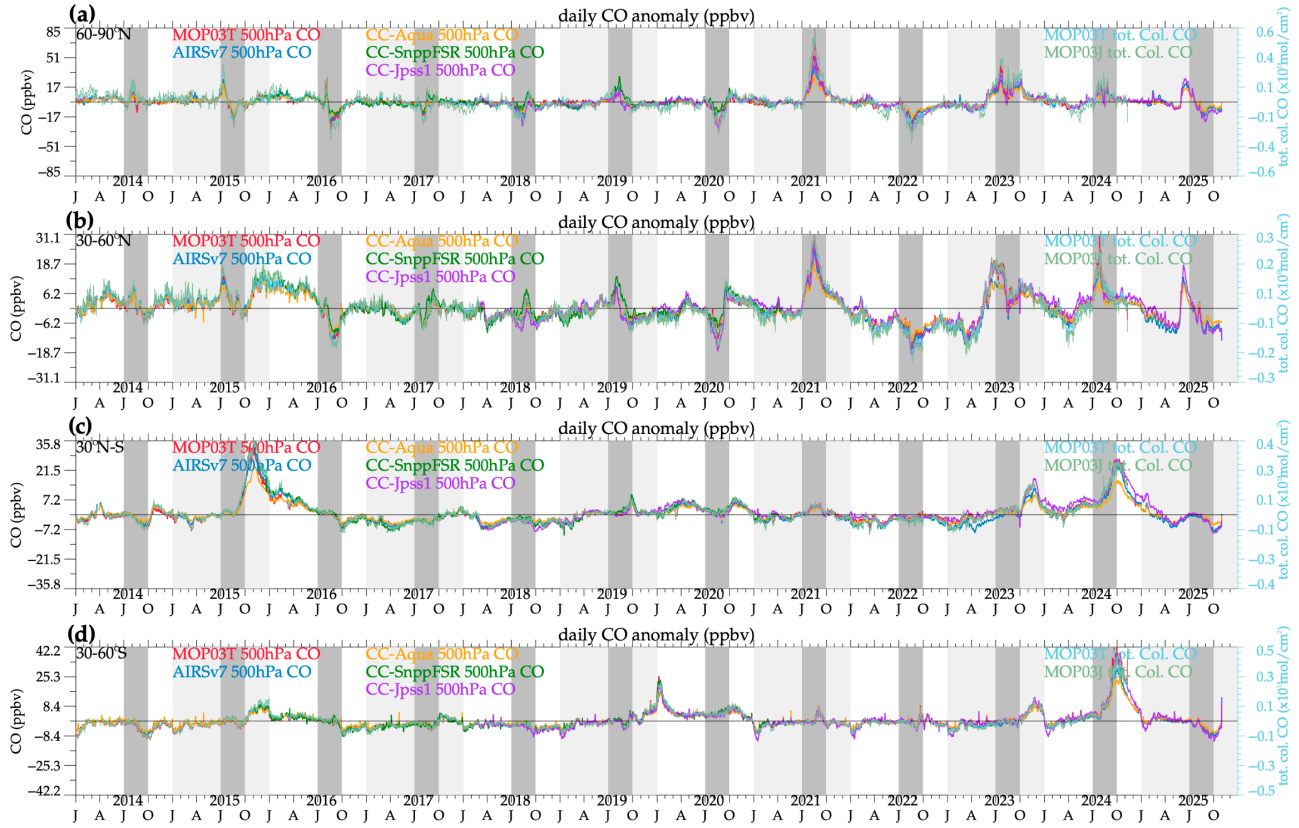

Figure 7. Interannual variability in 500 hPa CO for various latitude bands from MOPITT TIR (red), AIRS v7 (blue), CLIMCAPS-Aqua (orange), CLIMCAPS-SNPP FSR (green), and CLIMCAPS-JPSS1 FSR (purple) over 2014–2025 for (**a**) 60–90°N, (**b**) 30–60°N, (**c**) 30°N–S, and (**d**) 30–60°S. Mid-tropospheric CO anomalies align with known wildfire activity and mirror total column CO ($\times 10^{18}$ mol/cm^2, right *y*-axis) from MOPITT TIR (light blue) and TIR + NIR (light green). The interannual variabilities in CO are calculated by removing daily annual cycles between 2018 and 2023. For each year, labels "J", "A", "J", "O" on x-axis represents "January", "April", "July", and "October", respectively.

The nearly identical interannual variabilities in CO are further summarized in Table 2, which lists correlation coefficients between MOPITT TIR 500 hPa CO anomalies and four long records for 2014–2024: (1) AIRS 500 hPa CO anomalies, (2) CLIMCAPS-Aqua 500 hPa CO anomalies, (3) MOPITT TIR total-column CO anomalies, and (4) MOPITT TIR + NIR total-column CO anomalies. To reduce day-to-day variability and mitigate missing data, all time series are smoothed with a 30-day (approximately monthly) boxcar average. The correlation coefficients all exceed 0.93. In particular, the correlations between MOPITT TIR 500 hPa CO and MOPITT total-column CO, TIR, or TIR + NIR approach unity, indicating that variability at 500 hPa effectively represents the variability of the total-column CO.

Table 2. Correlation coefficients (R) between MOPITT TIR 500 hPa CO and four selected long records at different latitudes for the period of 2014–2024.

Datasets / Latitude Bands	AIRS v7 500 hPa CO	CC-Aqua 500 hPa CO	MOPITT TIR Column CO	MOPITT TIR + NIR Column CO
60–90°N	0.93	0.95	0.97	0.95
30–60°N	0.95	0.96	0.99	0.97
30°N-S	0.97	0.97	0.99	0.98
30–60°S	0.97	0.97	0.99	0.98

Taken together, these results demonstrate that the observed interannual variability in mid-tropospheric CO is robust across instruments and retrieval systems. The consistency

observed between AIRS and CrIS—despite differences in platform, spectral resolution, algorithms, and *a priori* assumptions—supports the feasibility of constructing a continuous, multidecadal CO record across these instruments. This gives us confidence to further study the long-term variability of CO from both the AIRS v7 and CLIMCAPS systems. The deployment of JPSS-4 (2027) and JPSS-3 (2032) will extend the CO records from the U.S. LEO platforms to more than 40 years. This continuity, in turn, is critical for monitoring the impacts of wildfire trends and understanding long-term changes in atmospheric composition.

4. More Frequent Wildfires

Over the past two decades, while anthropogenic CO emissions have declined in many parts of the world due to cleaner technologies and environmental regulations (e.g., [34,40]), satellite observations of carbon monoxide (CO) have shown the growing surge in CO emissions from biomass burning [30,40,41,57]. It has also been reported that fire seasons are becoming longer (e.g., [58]) and, in some years, even start earlier in the spring and extend into autumn due to warmer springs, longer summer dry seasons, and drier soils and vegetation. There have been marked increases in the frequency and intensity of wildfire over the past decade (e.g., [59,60]).

Changes in the high northern latitudes have been particularly extreme. Wildfire emissions from boreal forests in Eurasia and North America nearly tripled between 2001 and 2023, driven by a warmer, drier climate [9]. Figure 8a presents the AIRS 500 hPa CO anomaly averaged over 50–75°N. The elevated 500 hPa CO anomalies show the impacts of major wildfire events, including the 2010 Russian wildfires, 2012 California fires, Siberian fires in July to September 2021, and the most recent historic Canadian wildfires in 2023 [27,61] and 2024 [55]. MOPITT TIR 500 hPa CO and total column CO (right *y*-axis) are also overlaid in Figure 8a. The mid-tropospheric and total column quantities display strong agreement in the timing, duration, and magnitude of anomalous CO events.

To further highlight the connection between CO anomalies and wildfire activity, we examine correlations with two key fire indicators: surface vapor pressure deficit (VPD) from AIRS and the count of fire pixels from MODIS. AIRS surface VPD, defined as the differences between actual and saturation water vapor pressure, is a measure of the drying power of the atmosphere at the surface and is a critical predictor of wildfire risk [62]. Higher VPD values indicate drier conditions and increased vegetation flammability, both of which promote fire ignition and spread. MODIS global fire location product (MCD14ML) in collection 6 and 6.1, derived from Terra and Aqua satellites, provides the geographic coordinates and date of individual fire pixels [63].

Figure 8b shows corresponding AIRS v7 VPD anomalies in 50–75°N of the same period, further supporting the linkage between atmospheric dryness and fire-induced CO enhancements. Figure 8c shows MODIS total counts of fire pixels in the area. The Northern Hemisphere exhibits a notable increase in fire activity over this period, particularly in recent years. Moreover, the most recent wildfires after 2020 are apparently more prolonged than in earlier years. These three independent datasets consistently highlight the role of wildfire emissions in driving seasonal and interannual CO variability.

These results illustrate the role of wildfires in driving enhanced mid-tropospheric CO variability in the Northern Hemisphere. The alignment of CO, fire count, and VPD anomalies—both spatially and temporally—shows how climate-driven changes in fire behavior are increasingly shaping atmospheric composition. These trends of longer wildfire seasons and larger wildfire sizes are predicted to continue as more frequent and longer droughts occur [64]. Given the strength of the mid-tropospheric CO signal and its consistent

response across independent datasets, these satellites' observations serve as a valuable tool for monitoring global fire activity and its evolving impact on the atmosphere.

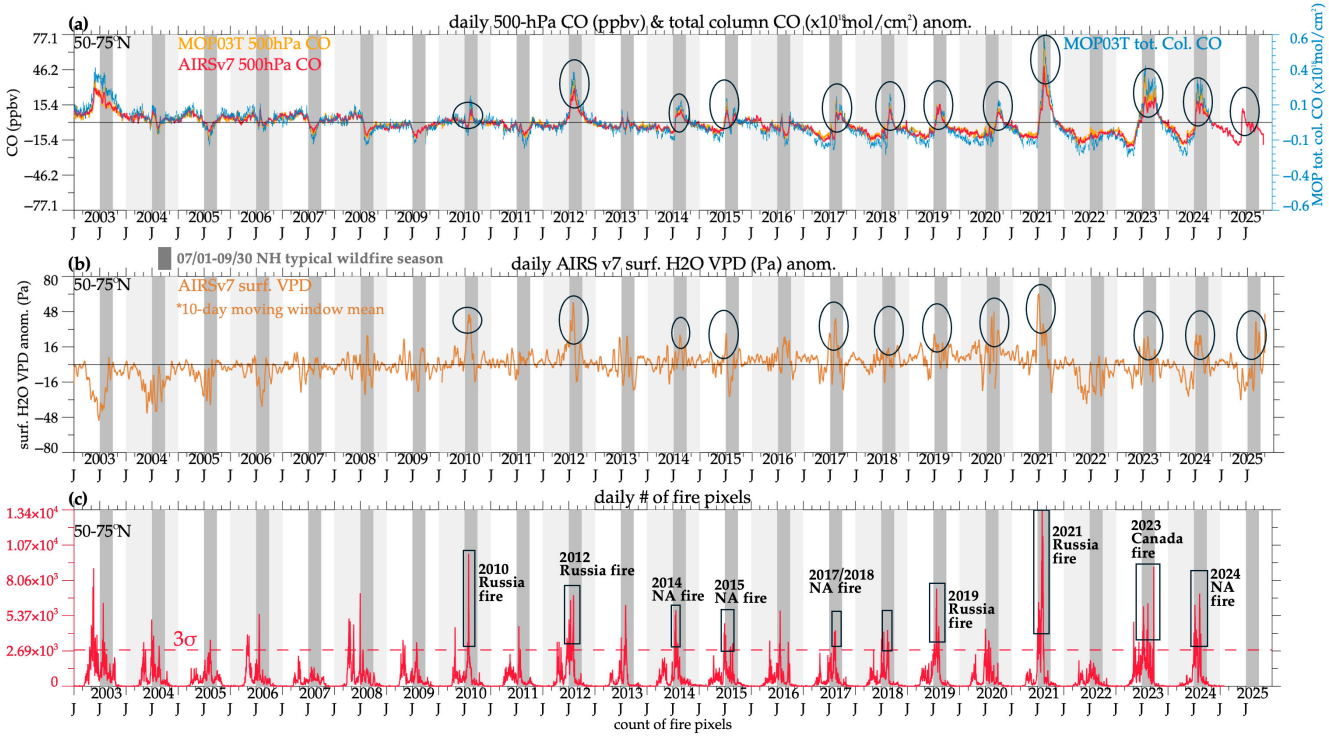

Figure 8. (**a**) The interannual variabilities in 500 hPa CO from AIRS v7 (red) and MOPITT TIR (orange), overlaid with MOPITT TIR total column CO (deep blue, right *y*-axis); compared to (**b**) anomalous AIRS v7 vapor pressure deficit (VPD), and (**c**) total number of fire pixels observed by MODIS (Aqua and Terra). The interannual variability in panels (**a**,**b**) is calculated by removing annual cycle 2005–2015. The ovals in panels (**a**,**b**) highlight where anomalously high CO coincides with anomalously high VPD; the rectangles in panel (**c**) mark the high counts of fire pixels matching with these high-CO/high-VPD anomalies. For each year, labels "J" and "J" on x-axis represents "January" and "July", respectively.

5. Conclusions & Further Discussion

Carbon monoxide (CO) plays a central role in atmospheric chemistry, acting as a key tracer for combustion emissions and as a precursor to tropospheric ozone. Long-term, consistent global observations of CO are therefore essential for monitoring pollution, understanding fire-driven atmospheric variability, and assessing the impacts of climate change on air quality.

Our results demonstrate that, despite differences in instrument design and spectral resolution (Figure 1), both the AIRS v7 and CLIMCAPS AIRS/CrIS CO products from different algorithms (Table 1) consistently capture the interannual variability in CO profiles (Figure 3). This agreement is particularly strong in the mid-troposphere, where both AIRS and CrIS instruments are most sensitive to CO (Figure 2). This implies that each dataset—-although different in absolute magnitudes (Figure 3)—exhibits a self-consistent climatology, so that it captures the interannual variability in CO vertical structures very well (Figure 4). Therefore, we see consistent records of extreme events well-captured by all AIRS/CrIS records (Figures 5–7). This finding is broadly consistent with previous studies that covered shorter time periods [34,40]. The close agreement between AIRS v7 and CLIMCAPS retrievals from AIRS and CrIS—particularly when evaluated against independent MOPITT measurements, both near the mid-troposphere (Figures 5 and 6) and for the total column (Figures 7 and 8)—highlights the robustness of these satellite products

for long-term CO monitoring (Table 2). The agreement also suggests that surface-level anthropogenic emissions play a relatively minor role in driving interannual CO variability at the global scale (Figures 4, 5, 7 and 8 and Table 2); instead, large-scale wildfires appear to be the dominant source of year-to-year CO anomalies (Figure 8).

Looking ahead, the CrIS sounder system offers a promising path toward continuing the multidecadal record of global CO. The Suomi National Polar-orbiting Partnership (SNPP) satellite, launched in 2011, was followed by the first and second Joint Polar Satellite System (JPSS) platforms in 2017 and 2022, respectively. JPSS-4 and JPSS-3 are scheduled for launch in 2027 and 2032, respectively, with mission lifetimes extending through at least 2045. As illustrated in Figure 9, when combined with the MOPITT and AIRS data, the current and planned CrIS observations will enable the construction of a contiguous CO record exceeding 40 years. The demonstrated agreement in CO variability across AIRS, CrIS, and MOPITT further strengthens the feasibility of building a long-term, climate-quality CO dataset.

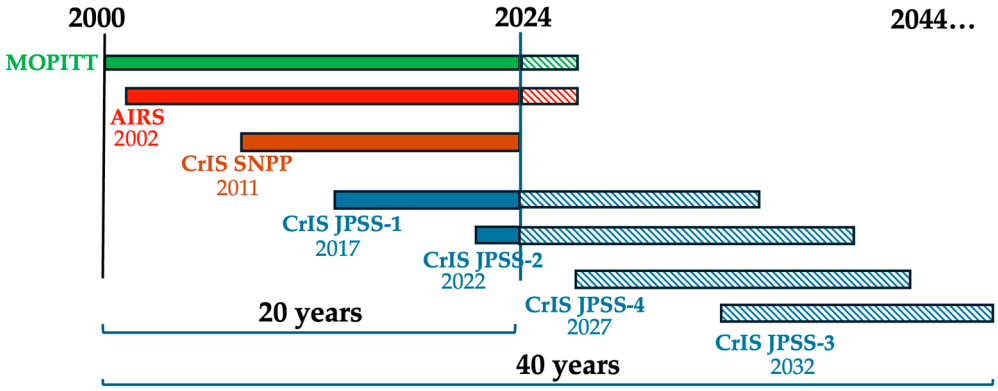

Figure 9. Timeline of thermal infrared CO observations from MOPITT, AIRS, and CrIS (SNPP and JPSS series). Shaded bars indicate mission lifetimes, with extensions in green showing potential mission overlap through 2045. Together, these datasets can provide over four decades of continuous global CO monitoring.

A 40+-year record of mid-tropospheric CO offers substantial scientific value. First, it enables the detection and attribution of trends in biomass burning and anthropogenic emissions across multiple continents. Second, it provides a critical benchmark for evaluating chemistry-climate models and reanalysis systems. Third, the data can be used to track shifts in fire regimes, vegetation flammability, and climate-induced changes in atmospheric transport. Together with continued observations from other international missions, the U.S.-based TIR CO records are placed to support atmospheric research, climate assessment, and environmental policy over the coming decades. To fully realize this vision, continued support for consistent retrieval algorithms, cross-platform validation, and data reprocessing will be essential.

Author Contributions: Conceptualization, T.W. and V.H.P.; Methodology, T.W. and V.H.P.; Software, T.W.; Validation, T.W.; Formal analysis, T.W. and V.H.P.; Investigation, T.W., V.H.P. and E.M.; Data curation, T.W. and E.M.; Writing—original draft, T.W.; Writing—review and editing, V.H.P., E.M., T.S.P., B.L. and R.M.; Visualization, T.W.; Supervision, V.H.P.; Project administration, T.S.P., B.L. and R.M.; Funding acquisition, T.S.P., B.L. and R.M. All authors have read and agreed to the published version of the manuscript.

Funding: This work was funded from the NASA Science Mission Directorate (SMD), Earth Science Division, under the Aqua Mission and the AIRS project. T.S.P. and T.W. were partially supported by NASA FireTech grant 80NM0023F0047; T.W. was partially supported by NASA grant NNH22ZDA001N-MEaSUREs.

Data Availability Statement: AIRS v7 IR-only L2 support retrievals (doi: 10.5067/APJ6EEN0PD0Z) can be accessed at https://disc.gsfc.nasa.gov/datasets/AIRS2SUP_7.0/summary (last accessed on 14 December 2025). CLIMCAPS-Aqua IR-only v2.1 L2 retrievals (doi: 10.5067/WZVJ68EXNLK7) can be accessed at https://disc.gsfc.nasa.gov/datasets/SNDRAQIL2CPS_2.1/summary?keywords=CLIMCAPS%20Aqua (last accessed on 14 December 2025); CLIMCAPS-SNPP FSR v2.1 L2 retrievals (doi: 10.5067/SD6WORV4GX8P) can be accessed at https://disc.gsfc.nasa.gov/datasets/SNDRSNIML2CPS_2.1/summary?keywords=CLIMCAPS%20Snpp (last accessed on 14 December 2025); and CLIMCAPS-JPSS1 FSR v2.1 L2 retrievals (doi: 10.5067/5GHJWKUXQSP6) can be accessed at https://disc.gsfc.nasa.gov/datasets/SNDRJ1IML2CPS_2.1/summary?keywords=CLIMCAPS%20JPSS1 (last accessed on 14 December 2025). MOPITT CO gridded daily means from thermal infrared (TIR) radiances (doi: 10.5067/TERRA/MOPITT/MOP03T.009, last accessed on 14 December 2025) and thermal and near infrared (JIR) combined retrievals (doi: 10.5067/TERRA/MOPITT/MOP03J.009, last accessed on 14 December 2025) in version 9 can be accessed at https://asdc.larc.nasa.gov/project/MOPITT/MOP03J_9 (last accessed on 14 December 2025). MODIS collection 6 monthly fire location product (MCD14ML) can be accessed via sftp from university of Maryland (https://modis-fire.umd.edu/files/MODIS_C6_Fire_User_Guide_B.pdf, last accessed on 14 December 2025).

Acknowledgments: This work was conducted at the Jet Propulsion Laboratory, California Institute of Technology, under a contract with the National Aeronautics and Space Administration (80NM0018D0004). ©2025. All rights reserved. The authors would like to acknowledge Nadia Smith and Chris Barnet for all their work and achievements in developing the CLIMCAPS algorithm, as well as the current and past members of the AIRS Science Team who have been responsible for the development of the AIRS v7 products. The authors would also like to thank Helen Worden for helpful discussions on the MOPITT products.

Conflicts of Interest: The authors declare no conflicts of interest.

References

1. Crutzen, P.J.; Heidt, L.E.; Krasnec, J.P.; Pollock, W.H.; Seiler, W. Biomass burning as a source of atmospheric gases CO, H_2, N_2O, NO, CH_3Cl and COS. *Nature* **1979**, *282*, 253–256. [CrossRef]
2. Jacob, D.J. *Introduction to Atmospheric Chemistry*; Princeton University Press: Princeton, NJ, USA, 1999.
3. Conte, L.; Szopa, S.; Séférian, R.; Bopp, L. The oceanic cycle of carbon monoxide and its emissions to the atmosphere. *Biogeosciences* **2019**, *16*, 881–902. [CrossRef]
4. Badr, O.; Probert, S.D. Sources of atmospheric carbon monoxide. *Appl. Energy* **1994**, *49*, 145–195. [CrossRef]
5. Bowman, K.P. Transport of carbon monoxide from the tropics to the extratropics. *J. Geophys. Res. Atmos.* **2006**, *111*, D02107. [CrossRef]
6. Edwards, D.P.; Emmons, L.K.; Gille, J.C.; Chu, A.; Attié, J.; Giglio, L.; Wood, S.W.; Haywood, J.; Deeter, M.N.; Massie, S.T.; et al. Satellite-observed pollution from Southern Hemisphere biomass burning. *J. Geophys. Res. Atmos.* **2006**, *111*, D14312. [CrossRef]
7. Park, M.; Randel, W.J.; Emmons, L.K.; Livesey, N.J. Transport pathways of carbon monoxide in the Asian summer monsoon diagnosed from Model of Ozone and Related Tracers (MOZART). *J. Geophys. Res. Atmos.* **2009**, *114*, D08303. [CrossRef]
8. Wang, T.; Randel, W.J.; Dessler, A.E.; Schoeberl, M.R.; Kinnison, D.E. Trajectory model simulations of ozone (O_3) and carbon monoxide (CO) in the lower stratosphere. *Atmos. Chem. Phys.* **2014**, *14*, 7135–7147. [CrossRef]
9. Jones, M.W.; Veraverbeke, S.; Andela, N.; Doerr, S.H.; Kolden, C.; Mataveli, G.; Pettinari, M.L.; Le Quéré, C.; Rosan, T.M.; van der Werf, G.R.; et al. Global rise in forest fire emissions linked to climate change in the extratropics. *Science* **2024**, *386*, eadl5889. [CrossRef]
10. Buchwitz, M.; de Beek, R.; Noël, S.; Burrows, J.P.; Bovensmann, H.; Schneising, O.; Khlystova, I.; Bruns, M.; Bremer, H.; Bergamaschi, P.; et al. Atmospheric carbon gases retrieved from SCIAMACHY by WFM-DOAS: Version 0.5 CO and CH_4 and impact of calibration improvements on CO_2 retrieval. *Atmos. Chem. Phys.* **2006**, *6*, 2727–2751. [CrossRef]
11. Borsdorff, T.; Aan de Brugh, J.; Hu, H.; Aben, I.; Hasekamp, O.; Landgraf, J. Measuring carbon monoxide with TROPOMI: First results and a comparison with ECMWF-IFS analysis data. *Geophys. Res. Lett.* **2018**, *45*, 2826–2832. [CrossRef]
12. Seinfeld, J.H.; Pandis, S.N. *Atmospheric Chemistry and Physics*; John Wiley and Sons: New York, NY, USA, 1998.
13. Reid, J.S.; Eck, T.F.; Christopher, S.A.; Koppmann, R.; Dubovik, O.; Eleuterio, D.P.; Holben, B.N.; Reid, E.A.; Zhang, J. A review of biomass burning emissions part III: Intensive optical properties of biomass burning particles. *Atmos. Chem. Phys.* **2005**, *5*, 827–849. [CrossRef]

14. Clerbaux, C.; Hadji-Lazaro, J.; Payan, S.; Camy-Peyret, C.; Mégie, G. Retrieval of CO columns from IMG/ADEOS spectra. *IEEE Trans. Geosci. Remote Sens.* **1999**, *37*, 1657–1661. [CrossRef]
15. Beer, R. TES on the Aura Mission: Scientific objectives, measurements, and analysis overview. *IEEE Trans. Geosci. Remote Sens.* **2006**, *44*, 1102–1105. [CrossRef]
16. McMillan, W.W.; Evans, K.D.; Barnet, C.D.; Maddy, E.S.; Sachse, G.W.; Diskin, G.S. Validating the AIRS Version 5 CO retrieval with DACOM in situ measurements during INTEX-A and -B. *IEEE Trans. Geosci. Remote Sens.* **2011**, *49*, 2802–2813. [CrossRef]
17. Smith, N.; Barnet, C.D. CLIMCAPS observing capability for temperature, moisture, and trace gases from AIRS/AMSU and CrIS/ATMS. *Atmos. Meas. Tech.* **2020**, *13*, 4437–4459. [CrossRef]
18. Smith, N.; Esmaili, R.; Barnet, C. Community Long-Term Infrared Microwave Combined Atmospheric Product System (CLIMCAPS) Science Application Guides. 2021. Available online: https://docserver.gesdisc.eosdis.nasa.gov/public/project/Sounder/CLIMCAPS_V2_L2_science_guides.pdf (accessed on 14 December 2025).
19. Worden, H.M.; Francis, G.L.; Kulawik, S.S.; Bowman, K.W.; Cady-Pereira, K.; Fu, D.; Hegarty, J.D.; Kantchev, V.; Luo, M.; Payne, V.H.; et al. TROPESS/CrIS carbon monoxide profile validation with NOAA GML and ATom in situ aircraft observations. *Atmos. Meas. Tech.* **2022**, *15*, 5383–5398. [CrossRef]
20. George, M.; Clerbaux, C.; Bouarar, I.; Coheur, P.-F.; Deeter, M.N.; Edwards, D.P.; Francis, G.; Gille, J.C.; Hadji-Lazaro, J.; Hurtmans, D.; et al. An examination of the long-term CO records from MOPITT and IASI: Comparison of retrieval methodology. *Atmos. Meas. Tech.* **2015**, *8*, 4313–4328. [CrossRef]
21. Barret, B.; Loicq, P.; Le Flochmoën, E.; Bennouna, Y.; Hadji-Lazaro, J.; Hurtmans, D.; Sauvage, B. Validation of 12 years (2008–2019) of IASI-A CO with IAGOS aircraft observations. *Atmos. Meas. Tech.* **2025**, *18*, 129–149. [CrossRef]
22. Zeng, Z.C. Global carbon monoxide retrieval from the hyperspectral infrared atmospheric sounder-II onboard FengYun-3E in a dawn-dusk sun-synchronous orbit. *J. Quant. Spectrosc. Radiat. Transf.* **2025**, *333*, 109336. [CrossRef]
23. Zeng, Z.-C.; Lee, L.; Qi, C. Diurnal carbon monoxide observed from a geostationary infrared hyperspectral sounder: First result from GIIRS on board FengYun-4B. *Atmos. Meas. Tech.* **2023**, *16*, 3059–3083. [CrossRef]
24. Grandell, J.; Stuhlmann, R. Limitations to a Geostationary Infrared Sounder due to Diffraction: The Meteosat Third Generation Infrared Sounder (MTG IRS). *J. Atmos. Ocean. Technol.* **2007**, *24*, 1740–1749. [CrossRef]
25. Naus, S.; Domingues, L.G.; Krol, M.; Luijkx, I.T.; Gatti, L.V.; Miller, J.B.; Gloor, E.; Basu, S.; Correia, C.; Koren, G.; et al. Sixteen years of MOPITT satellite data strongly constrain Amazon CO fire emissions. *Atmos. Chem. Phys.* **2022**, *22*, 14735–14750. [CrossRef]
26. Griffin, D.; Chen, J.; Anderson, K.; Makar, P.; McLinden, C.A.; Dammers, E.; Fogal, A. Biomass burning CO emissions: Exploring insights through TROPOMI-derived emissions and emission coefficients. *Atmos. Chem. Phys.* **2024**, *24*, 10159–10186. [CrossRef]
27. Byrne, B.; Liu, J.; Bowman, K.W.; Pascolini-Campbell, M.; Chatterjee, A.; Pandey, S.; Miyazaki, K.; van der Werf, G.R.; Wunch, D.; Wennberg, P.O.; et al. Carbon emissions from the 2023 Canadian wildfires. *Nature* **2024**, *633*, 835–839. [CrossRef]
28. Marey, H.S.; Drummond, J.R.; Jones, D.B.A.; Worden, H.; Clerbaux, C.; Borsdorff, T.; Gille, J. A comparative analysis of satellite-derived CO retrievals during the 2020 wildfires in North America. *J. Geophys. Res. Atmos.* **2024**, *129*, e2023JD039876. [CrossRef]
29. Buchholz, R.R.; Park, M.; Worden, H.M.; Tang, W.; Edwards, D.P.; Gaubert, B.; Deeter, M.N.; Sullivan, T.; Ru, M.; Chin, M.; et al. New seasonal pattern of pollution emerges from changing North American wildfires. *Nat. Commun.* **2022**, *13*, 2043. [CrossRef]
30. Yurganov, L.; Rakitin, V. Two Decades of Satellite Observations of Carbon Monoxide Confirm the Increase in Northern Hemispheric Wildfires. *Atmosphere* **2022**, *13*, 1479. [CrossRef]
31. Hedelius, J.K.; Toon, G.C.; Buchholz, R.R.; Iraci, L.T.; Podolske, J.R.; Roehl, C.M.; Wennberg, P.O.; Worden, H.M.; Wunch, D. Regional and urban column CO trends and anomalies as observed by MOPITT over 16 years. *J. Geophys. Res. Atmos.* **2021**, *126*, e2020JD033967. [CrossRef]
32. Miyazaki, K.; Sekiya, T.; Fu, D.; Bowman, K.W.; Kulawik, S.S.; Sudo, K.; Walker, T.; Kanaya, Y.; Takigawa, M.; Ogochi, K.; et al. Balance of emission and dynamical controls on ozone during the Korea-United States Air Quality campaign from multiconstituent satellite data assimilation. *J. Geophys. Res. Atmos.* **2019**, *124*, 387–413. [CrossRef]
33. Gaubert, B.; Edwards, D.P.; Anderson, J.L.; Arellano, A.F.; Barré, J.; Buchholz, R.R.; Darras, S.; Emmons, L.K.; Fillmore, D.; Granier, C.; et al. Global Scale Inversions from MOPITT CO and MODIS AOD. *Remote Sens.* **2023**, *15*, 4813. [CrossRef]
34. Buchholz, R.R.; Worden, H.M.; Park, M.; Francis, G.; Deeter, M.N.; Edwards, D.P.; Emmons, L.K.; Gaubert, B.; Gille, J.; Martínez-Alonso, S.; et al. Air pollution trends measured from Terra: CO and AOD over industrial, fire-prone, and background regions. *Remote Sens. Environ.* **2021**, *256*, 112275. [CrossRef]
35. Chahine, M.T.; Pagano, T.S.; Aumann, H.H.; Atlas, R.; Barnet, C.; Blaisdell, J.; Chen, L.; Divakarla, M.; Fetzer, E.J.; Goldberg, M.; et al. Improving Weather Forecasting and Providing New Data on Greenhouse Gases. *AIRS. Bull. Am. Meteor. Soc.* **2006**, *87*, 911–926. [CrossRef]

36. McMillan, W.W.; Barnet, C.; Strow, L.; Chahine, M.T.; McCourt, M.L.; Warner, J.X.; Novelli, P.C.; Korontzi, S.; Maddy, E.S.; Datta, S. Daily global maps of carbon monoxide from NASA's Atmospheric Infrared Sounder. *Geophys. Res. Lett.* **2005**, *32*, L11801. [CrossRef]
37. Wang, T.; Payne, V.; Manning, E.; Yue, Q.; Wong, S.; Lambrigtsen, B.H.; Fetzer, E.; Monarrez, R.; Pagano, T.; Fishbein, E.; et al. *Testing Report for the AIRS v7 and CLIMCAPS-Aqua v2 Level-3 Monthly Gridded Composition Products*; Jet Propulsion Laboratory/California Institute of Technology: La Cañada Flintridge, CA, USA, 2022. [CrossRef]
38. Wang, T.; Payne, V.; Manning, E.; Wong, S.; Yue, Q.; Lambrigtsen, B.H.; Fetzer, E.; Monarrez, R. *Test Report of AIRS v7 and CLIMCAPS-Aqua v02.39 Level-2 Carbon Monoxide (CO) Profiles*; Jet Propulsion Laboratory/California Institute of Technology: La Cañada Flintridge, CA, USA, 2024. [CrossRef]
39. Warner, J.; Comer, M.M.; Barnet, C.D.; McMillan, W.W.; Wolf, W.; Maddy, E.; Sachse, G. A comparison of satellite tropospheric carbon monoxide measurements from AIRS and MOPITT during INTEX-A. *J. Geophys. Res. Atmos.* **2007**, *112*, D12S17. [CrossRef]
40. Worden, H.M.; Deeter, M.N.; Frankenberg, C.; George, M.; Nichitiu, F.; Worden, J.; Aben, I.; Bowman, K.W.; Clerbaux, C.; Coheur, P.F.; et al. Decadal record of satellite carbon monoxide observations. *Atmos. Chem. Phys.* **2013**, *13*, 837–850. [CrossRef]
41. Zhang, X.; Liu, J.; Han, H.; Zhang, Y.; Jiang, Z.; Wang, H.; Meng, L.; Li, Y.C.; Liu, Y. Satellite-Observed Variations and Trends in Carbon Monoxide over Asia and Their Sensitivities to Biomass Burning. *Remote Sens.* **2020**, *12*, 830. [CrossRef]
42. van Der Werf, G.R.; Randerson, J.T.; Giglio, L.; Van Leeuwen, T.T.; Chen, Y.; Rogers, B.M.; Mu, M.; Van Marle, M.J.; Morton, D.C.; Collatz, G.J.; et al. Global fire emissions estimates during 1997–2016. *Earth Syst. Sci. Data* **2017**, *9*, 697–720. [CrossRef]
43. Susskind, J.; Barnet, C.D.; Blaisdell, J.M. Retrieval of atmospheric and surface parameters from AIRS/AMSU/HSB data in the presence of clouds. *IEEE Trans. Geosci. Remote Sens.* **2003**, *41*, 390–409. [CrossRef]
44. Warner, J.X.; Wei, Z.; Strow, L.L.; Barnet, C.D.; Sparling, L.C.; Diskin, G.; Sachse, G. Improved agreement of AIRS tropospheric carbon monoxide products with other EOS sensors using optimal estimation retrievals. *Atmos. Chem. Phys.* **2010**, *10*, 9521–9533. [CrossRef]
45. Smith, N.; Barnet, C.D. CLIMCAPS—A NASA long-term product for infrared + microwave atmospheric soundings. *Earth Space Sci.* **2023**, *10*, e2022EA002701. [CrossRef]
46. Irion, F.W.; Kahn, B.H.; Schreier, M.M.; Fetzer, E.J.; Fishbein, E.; Fu, D.; Kalmus, P.; Wilson, R.C.; Wong, S.; Yue, Q. Single-footprint retrievals of temperature, water vapor and cloud properties from AIRS. *Atmos. Meas. Tech.* **2018**, *11*, 971–995. [CrossRef]
47. Kulawik, S.S.; Worden, J.R.; Payne, V.H.; Fu, D.; Wofsy, S.C.; McKain, K.; Sweeney, C.; Daube, B.C., Jr.; Lipton, A.; Polonsky, I.; et al. Evaluation of single-footprint AIRS CH_4 profile retrieval uncertainties using aircraft profile measurements. *Atmos. Meas. Tech.* **2021**, *14*, 335–354. [CrossRef]
48. Hegarty, J.D.; Cady-Pereira, K.E.; Payne, V.H.; Kulawik, S.S.; Worden, J.R.; Kantchev, V.; Worden, H.M.; McKain, K.; Pittman, J.V.; Commane, R.; et al. Validation and error estimation of AIRS MUSES CO profiles with HIPPO, ATom, and NOAA GML aircraft observations. *Atmos. Meas. Tech.* **2022**, *15*, 205–223. [CrossRef]
49. Anderson, G.P.; Clough, S.A.; Kneizys, F.X.; Chetwynd, J.H.; Shettle, E.P. *AFGL Atmospheric Constituent Profiles (0.120 km)*; Technical Report AFGL–TR–86–0110; Air Force Geophysics Lab Hanscom AFB: Bedford, MA, USA, 1986.
50. Gambacorta, A.; Barnet, C.; Wolf, W.; King, T.; Maddy, E.; Strow, L.; Xiong, X.; Nalli, N.; Goldberg, M. An Experiment Using High Spectral Resolution CrIS Measurements for Atmospheric Trace Gases: Carbon Monoxide Retrieval Impact Study. *IEEE Geosci. Remote Sens. Lett.* **2014**, *11*, 1639–1643. [CrossRef]
51. Deeter, M.N.; Martínez-Alonso, S.; Edwards, D.P.; Emmons, L.K.; Gille, J.C.; Worden, H.M.; Pittman, J.V.; Daube, B.C.; Wofsy, S.C. Validation of MOPITT Version 5 thermal-infrared, near-infrared, and multispectral carbon monoxide profile retrievals for 2000–2011. *J. Geophys. Res.* **2013**, *118*, 6710–6725. [CrossRef]
52. Deeter, M.; Francis, G.; Gille, J.; Mao, D.; Martínez-Alonso, S.; Worden, H.; Ziskin, D.; Drummond, J.; Commane, R.; Diskin, G.; et al. The MOPITT Version 9 CO product: Sampling enhancements and validation. *Atmos. Meas. Tech.* **2022**, *15*, 2325–2344. [CrossRef]
53. Hoesly, R.; Smith, S.J.; Prime, N.; Ahsan, H.; Suchyta, H.; O'Rourke, P.; Crippa, M.; Klimont, Z.; Guizzardi, D.; Behrendt, J.; et al. *CEDS v_2024_07_08 Release Emission Data (v_2024_07_08) [Data Set]*; Zenodo: Geneva, Switzerland, 2024. [CrossRef]
54. Field, R.D.; van der Werf, G.R.; Fanin, T.; Fetzer, E.J.; Fuller, R.; Jethva, H.; Levy, R.; Livesey, N.J.; Luo, M.; Torres, O.; et al. Indonesian fire activity and smoke pollution in 2015 show persistent nonlinear sensitivity to El Niño-induced drought. *Proc. Natl. Acad. Sci. USA* **2016**, *113*, 9204–9209. [CrossRef]
55. Sobreira, E.; Lázaro, W.L.; Vitorino, B.D.; da Frota, A.V.B.; Young, C.E.F.; de Souza Campos, D.V.; Viana, C.R.S.; de Oliveira, E.; López-Ramirez, L.; de Souza, A.R.; et al. Wildfires and their toll on Brazil: Who's counting the cost? *Perspect. Ecol. Conserv.* **2025**, *23*, 214–217. [CrossRef]
56. Zheng, B.; Ciais, P.; Chevallier, F.; Yang, H.; Canadell, J.G.; Chen, Y.; van der Velde, I.R.; Aben, I.; Chuvieco, E.; Davis, S.J.; et al. Record-High CO_2 Emissions from Boreal Fires in 2021. *Science* **2023**, *379*, 912–917. [CrossRef]

57. Petetin, H.; Sauvage, B.; Parrington, M.; Clark, H.; Fontaine, A.; Athier, G.; Blot, R.; Boulanger, D.; Cousin, J.-M.; Nédélec, P.; et al. The role of biomass burning as derived from the tropospheric CO vertical profiles measured by IAGOS aircraft in 2002–2017. *Atmos. Chem. Phys.* **2018**, *18*, 17277–17306. [CrossRef]
58. Jolly, W.M.; Cochrane, M.A.; Freeborn, P.H.; Holden, Z.A.; Brown, T.J.; Williamson, G.J.; Bowman, D.M.J.S. Climate-induced variations in global wildfire danger from 1979 to 2013. *Nat. Commun.* **2015**, *6*, 7537. [CrossRef] [PubMed]
59. Wilmot, T.Y.; Mallia, D.V.; Hallar, A.G.; Lin, J.C. Wildfire plumes in the Western US are reaching greater heights and injecting more aerosols aloft as wildfire activity intensifies. *Sci. Rep.* **2022**, *12*, 12400. [CrossRef] [PubMed]
60. Cunningham, C.X.; Williamson, G.J.; Bowman, D.M.J.S. Increasing frequency and intensity of the most extreme wildfires on Earth. *Nat. Ecol. Evol.* **2024**, *8*, 1420–1425. [CrossRef]
61. Lai, G.; Zhang, Y. Increased atmospheric aridity and reduced precipitation drive the 2023 extreme wildfire season in Canada. *Geophys. Res. Lett.* **2025**, *52*, e2024GL114492. [CrossRef]
62. Behrangi, A.; Fetzer, E.J.; Granger, S.L. Early detection of drought onset using near surface temperature and humidity observed from space. *Int. J. Remote Sens.* **2016**, *37*, 3911–3923. [CrossRef]
63. Giglio, L.; Schroeder, W.; Justice, C.O. The collection 6 MODIS active fire detection algorithm and fire products. *Remote Sens. Environ.* **2016**, *178*, 31–41. [CrossRef] [PubMed]
64. Ostoja, S.M.; Crimmins, A.R.; Byron, R.G.; East, A.E.; Méndez, M.; O'Neill, S.M.; Peterson, D.L.; Pierce, J.R.; Raymond, C.; Tripati, A.; et al. Focus on western wildfires. In *Fifth National Climate Assessment*; USGCRP (U.S. Global Change Research Program): Washington, DC, USA, 2023. [CrossRef]

Disclaimer/Publisher's Note: The statements, opinions and data contained in all publications are solely those of the individual author(s) and contributor(s) and not of MDPI and/or the editor(s). MDPI and/or the editor(s) disclaim responsibility for any injury to people or property resulting from any ideas, methods, instructions or products referred to in the content.